The relationship between extra-tropical cyclone intensity and precipitation in idealised current and future climates

Victoria A. Sinclair[1] and Jennifer L. Catto[2]

[1]Institute for Atmospheric and Earth System Research / Physics, Faculty of Science, University of Helsinki, PO BOX 64, FI-00014
[2]Faculty of Environment, Science and Economy, University of Exeter, Exeter, United Kingdom

Correspondence: Victoria Sinclair (victoria.sinclair@helsinki.fi)

Abstract. Extra-tropical cyclones (ETCs) are the main cause of precipitation in the mid-latitudes and there is substantial evidence that ETC-related precipitation will increase in the future. However, little is known about how this will impact on the dynamical strength of ETCs, and whether the impact will differ for different types of ETCs. Therefore, we quantify the relationship between maximum vorticity and ETC related precipitation in the current and idealised future climates, and also

5 determine how this relationship depends on the structure and characteristics of the ETC. Three 10-year long aqua-planet simulations are performed with a state-of-the-art global model, OpenIFS, that differ in their specified SST distributions, which are held fixed in time. A control simulation, a uniform warming simulation and a polar amplification simulation are performed. ETCs are objectively identified using the feature tracking software TRACK and k-means clustering is applied to the ETC precipitation field to group the ETCs into clusters with similar precipitation structures. In all experiments, ETCs with stronger

10 maximum vorticity are associated with more precipitation and this relationship is strongest in the uniform warming simulation and weakest in the control simulation. The differing slopes indicate that the increased precipitation in the warmer simulations does not feedback, via diabatic heating and potential vorticity anomalies, onto the dynamical intensity of the ETCs. The k-means clustering identifies four distinct and physically realistic types of ETCs which are present in all experiments meaning that the precipitation patterns associated with ETCs are unlikely to change in the future. The strongest relationship between

15 ETC maximum vorticity and precipitation occurs for ETCs that have most precipitation associated with the warm front. ETCs with the heaviest precipitation along the cold front, which are the most intense storms in terms of maximum voricity, also exhibit a strong relationship between maximum vorticity and precipitation but this is weaker and with more spread than the warm front ETCs, potentially due to more convective precipitation. Not all ETC types have a strong relationships between maximum vorticity and precipitation. ETCs located at high latitudes with weak precipitation have a weak relationship due to

20 the lack of moisture whereas ETCs with the precipitation located mainly in the centre of the ETCs have the weakest relation which is likely due to the lack of upper level forcing. These results stress that despite small changes in the strength of the cyclones, the precipitation increases are large, indicating potential future increases in flooding associated with cyclones.

1 Introduction

Extra-tropical cyclones (ETC) constitute a large part of the Earth's circulation, transporting energy and momentum poleward. These weather systems are also the dominant cause of day-to-day weather in the mid-latitudes. Hawcroft et al. (2012) showed that the majority of precipitation (70 - 80%) in the mid-latitude storm track regions is associated with ETCs and Pfahl and Wernli (2012) found that ETCs are responsible for a high percentage of precipitation extremes. Some, but not all, ETCs can have extremely large amounts of precipitation associated with them which can lead to flooding and thus to significant societal and economic impact. Therefore, it is important to understand what controls the amount of precipitation related to ETCs and how ETC related precipitation may change in the future.

ETCs have been extensively studied over the past century starting from Bjerknes (1919) and Bjerknes and Solberg (1922) who developed the well-know Norwegian model, a conceptual model of the structure of ETCs. Even from these early studies it has been known that precipitation develops in ETCs in regions where air is ascending which typically occurs along the frontal zones. Climatological studies of the occurrence of fronts have found that in the main storm track regions, up to 80% of the total precipitation can be associated with fronts (Catto et al., 2012), and an even larger proportion of extreme precipitation events (Catto and Pfahl, 2013). These exact proportions depend on the front identification and dataset used, but indicate the importance of these features.

The warm conveyor belt (WCB), a coherent ascending air stream which originates in the boundary layer of the warm sector of ETCs, was first described by Browning (1971), Harrold (1973) and Carlson (1980) and is also known to be a source of precipitation in ETCs. Using a climatology of WCBs developed using the ERA-Interim reanalysis dataset (Madonna et al., 2014), Pfahl et al. (2014) showed that 70–80% of precipitation extremes in some regions are associated with the WCB airstream. This feature, when associated with fronts, also gives a higher chance of an extreme precipitation event (Catto et al., 2015). Ascent in the warm conveyor belt is forced by warm air-advection but is also enhanced by diabatic heating. This diabatic heating can also influence the cyclone dynamics via the production of a low-level positive potential vorticity anomaly, which develops below the localised maximum in diabatic heating. This positive PV anomaly can potentially feedback onto the intensity of the ETC by enhancing the low-level circulation and thus the intensity of the ETCs. Binder et al. (2016) used a classification method to show that the WCB flow can contribute to rapid intensification of extratropical cyclones, but only in situations where there is strong enough upper-level forcing.

ETC intensity and the associated precipitation are strongly linked. We expect to see more precipitation in strong ETCs where there is strong forcing for ascent (Milrad et al., 2010; Dai and Nie, 2020). Field and Wood (2007) combined satellite observations with mean sea level pressure (MSLP) from reanalysis to understand how ETC precipitation and cloudiness depend on ETC strength and moisture availability. They found that precipitation increases with both ETC strength (as quantified by the mean surface wind speed within a 2000 km radius) and moisture, but that the deepest cyclones in terms of MSLP do not produce the most precipitation despite having the strongest winds. Pfahl and Sprenger (2016), using ERA-Interim reanalysis data, also found a strong relationship between ETC strength (in terms of wind speeds) and precipitation but also noted that this relationship varied strongly with latitude, with a very weak relationship at high latitudes, due to limitations in

moisture availability. They also showed that the relationship between precipitation and intensity was strongest when looking at the precipitation from 12 hours prior to the maximum intensity. This result, that maximum precipitation occurs before the maximum intensity of the ETC, is supported by Booth et al. (2018) who found that the maximum vorticity of an ETC occurred after the precipitation maximum in most ETCs (>70%), while only 20% of ETCs had their precipitation maximum after the vorticity maximum. Owen et al. (2021) focused on extremes (including both precipitation and winds and their co-occurrence) and found that ETCs associated with the extremes tend to have higher intensity than those that are not associated with extremes. Additionally, larger footprints of extreme events within cyclones are found for higher intensity cyclones (Owen et al., in prep).

Associated with the increased moisture due to the higher temperatures projected in the future, precipitation intensity (especially that of extremes) is expected to increase (Held and Soden, 2006). Many studies have shown this is also the case for ETC-related precipitation. For example, Zhang and Colle (2018) analysed ETCs in eastern North America and the western Atlantic in 10 models from phase 5 of the Coupled Model Intercomparison Project (CMIP5) and found that ETC-related precipitation increases by up to 30% between the historical and future climate simulations. Michaelis et al. (2017), in regional pseudo global warming experiments, also found ETC precipitation increases in a warmer climate while Hawcroft et al. (2018) showed that the number of ETCs with extreme precipitation associated with them may triple by the end of the century. Kodama et al. (2019) performed two high resolution global climate model simulations; one current climate and a future climate simulation and found that precipitation associated with intense ETCs increases at 7% / 1 K warming, whereas when all ETCs are considered, precipitation increases only at 3% / 1K warming. Similar results were also found by Reboita et al. (2021) for Southern Hemisphere ETCs when regional climate model simulations were analysed. Yettella and Kay (2017) analysed a large ensemble of climate model simulations and found that most of the increase in the intensity of precipitation associated with ETCs resulted from the thermodynamic effect of increased temperature, rather than a dynamical effect. Studies have also suggested that as well as an increase in ETC precipitation intensity in the future, the size of the cyclones and the area of the precipitation may increase (Reboita et al., 2021; Dai and Nie, 2022)

Climate change is expected to impact on the intensity of ETCs themselves. While the distribution of ETC intensities is not projected to change much (Priestley and Catto, 2022) even in high-emissions scenarios, the extreme ETCs are projected to increase in intensity in terms of vorticity, maximum wind speeds, and the footprint of high wind speeds (Pfahl et al., 2015; Sinclair et al., 2020; Priestley and Catto, 2022; Dolores-Tesillos et al., 2022). Forcing from latent heat release is projected to become more important for the ETC intensification in the future (Sinclair et al., 2020; Binder et al., 2022), indicating a role for precipitation intensification in the increase in cyclone intensity.

Idealised models have been used extensively in the past to understand cyclone dynamics (Simmons and Hoskins, 1978; Thorncroft et al., 1993) and, more recently, to understand ETC dynamics, precipitation and intensity in a warming climate. Two idealised modelling approaches have been used to study how ETCs response to a warmer climate, the first is baroclinic life cycle experiments (e.g. Boutle et al., 2011; Kirshbaum et al., 2018; Rantanen et al., 2019) and the second is aquaplanet simulations (e.g. Kodama et al., 2014; Pfahl et al., 2015; Sinclair et al., 2020). Both modelling approaches offer advantages over fully complex models, being able to better identify physical mechanisms for changes in ETCs. In this study we employ an aquaplanet model configuration, and include full physics, as previously used in Sinclair et al. (2020). This setup allows for a full

range of ETCs to develop (e.g. Catto, 2016), while removing complexities associated with land-sea contrasts of temperature, moisture, and surface drag.

It is clear that ETC-related precipitation is projected to increase in intensity in the future. A question remains as to whether this will impact will be on the dynamical strength of the cyclones. In other words, it is unclear how the relationship between precipitation and intensity might change in the future. Furthermore, there are many different dynamical structures of extratropical cyclones (e.g. Evans et al., 1994; Sinclair and Revell, 2000; Catto, 2016, 2018; Binder et al., 2022) and how this relationship depends on the type of ETC has yet to be quantified. Booth et al. (2018) used a subsetting method to group similar cyclones according to their precipitable water, and we will take a related approach by applying a clustering method to the precipitation structure to group ETCs. Using idealized aquaplanet simulations of a control climate, a uniform global warming scenario, and an Arctic amplification scenario, we will determine potential future changes in the cyclones and associated precipitation in the different cyclone clusters.

The questions we aim to address in this research are:

1. What is the relationship between precipitation intensity and cyclone intensity in the current and potential future climates?

2. How does the relationship between cyclone precipitation and cyclone intensity depend on the type of cyclone?.

3. How does the variability of precipitation structures associated with extratropical cyclones change in the future climate, and are certain types of cyclones more or less common?

Section 2 describes the numerical model, OpenIFS, that we use and the set up of the simulations that are performed. The methods used to analysis the output from these simulations are described in section 3. In section 4, the basic climatology of the three simulations is described before the relationship between precipitation and cyclone intensity is discussed in section 5. An analysis of the different types of ETCs that occur is presented in section 6 and how the relationship between precipitation and ETC intensity depends on the type of ETC is presented in section 7. Conclusions are presented in section 8.

2 Model Simulations

2.1 OpenIFS

The numerical simulations are performed with the state-of-the-art global numerical weather prediction model, OpenIFS Cy43r3v1. OpenIFS is a version of the Integrated Forecast System (IFS) used operationally at the European Centre for Medium Range Weather Forecasts (ECMWF). The dynamical core and the physical parameterizations in OpenIFS are identical to those in the same cycle of the full IFS. However, unlike the IFS, OpenIFS does not include the data assimilation package nor is it coupled to an ocean model. OpenIFS is available under licence to academic and research institutions. The equivalent version of the IFS (Cy43r3) to the version of OpenIFS used in these simulations was operational between July 2017 and June 2018. The complete documentation of IFS Cy43r3 is available online at https://www.ecmwf.int/en/publications/ifs-documentation

2.2 OpenIFS simulations

The numerical experiments conducted in this study utilise OpenIFS configured as an aquaplanet in which there is no land and the surface of the Earth is completely covered by ocean. Three simulations are performed and all are initialised from a real atmospheric state selected at random. However, some modifications are required to make the initial conditions suitable for an aqua-planet simulation. First, the land-sea mask is modified to be zero (ocean) everywhere and the surface geopotential is also set to zero. The atmospheric states are then interpolated to the new, flat surface. Surface pressure is also adjusted to reflect the removal of surface topography. All simulations have a diurnal cycle in incoming radiation but no annual cycle. During the simulations the incoming solar radiation is fixed at the equinoctial value and is thus symmetric about the Equator. The simulations are all run for 11 years and the first year of simulation is discarded to account for model spin-up. Output fields are written every 6 hours. The simulations are all run at a horizontal resolution of T255 (approximately 80 km) and have 60 model levels between the surface and the model top at 0.1 hPa.

The three aquaplanet simulations performed only differ from each other in terms of their prescribed sea surface temperature (SST) distributions (Fig. 1). In each experiment, the SST distribution is analytically specified as only a function of latitude and the SSTs are held constant through the simulation. The simulations represent a control, a case of uniform warming, and a case of polar amplification. The control simulation uses the QObs SST distribution proposed by Neale and Hoskins (2000). The SST distribution in the uniform warming simulation (referred to as SST4) is the QObs distribution but warmed everywhere by 4 K. The polar amplification simulation uses the QObs SST distribution between 45°S and 45°N and polewards of these latitudes, the SSTs are set to 5 °C.

Similar aquaplanet experiments have previously been presented by Sinclair et al. (2020). A few minor differences exist between the simulations presented here and those previous simulation. Firstly, the version of OpenIFS differs (Cy43r3 versus Cy 40r1), the horizontal resolution differs (T255 versus T159) and lastly, Sinclair et al. (2020) did not modify the surface pressure and therefore have lower climatological values of surface pressure than in this study.

3 Analysis methods

3.1 Cyclone Tracking

In all experiments, extra-tropical cyclones (ETCs) are objectively identified and tracked using TRACK (Hodges, 1994, 1995). ETCs are identified as localised maxima in the 850-hPa relative vorticity field truncated to T42 spectral resolution. Wave numbers smaller than wave number 5 are also set to zero to remove planetary scale features. Six-hourly input data is used to identify the ETC tracks. Initially, all ETCs in the Northern Hemisphere are identified, however to ensure that only synoptic-scale and mobile ETCs are retained for analysis we only retain ETC tracks that last for at least 2 days and travel 1000 km. To remove weak ETCs, tracks with a maximum T42 850-hPa relative vorticity of less than $1 \times 10^{-5} \text{s}^{-1}$ are also excluded from the analysis. Similar filtering has been applied in many other studies that employ TRACK (e.g. Dacre and Gray, 2009; Hodges

et al., 2011; Priestley et al., 2020). In addition to these standard filters, we also require that ETCs reach their maximum vorticity at a latitude north of 30°N and exist 24 hours before the time of maximum intensity.

3.2 Cyclone composites

Following the same method as Catto et al. (2010) and Dacre et al. (2012), composites of a range of meteorological variables are computed for the ETCs at different offset times relative to the time of maximum vorticity (t=0 hr). Negative offset times indicate that the composite is valid before the time of maximum intensity and hence when the ETC is intensifying. In contrast, positive offset times mean that the composite is valid during the decaying part of the ETC lifecycle. The first step in creating the composites is to select which ETCs to include in the composite. Previous studies have often select the strongest 50 - 200 ETCs or have selected the subset of ETCs to be composited by considering their geographic location. Here we create composites of different types of ETCs based on their precipitation patterns as identified by k-means clustering (more details in section 3.3). The second step in creating the composites is to regrid the meteorological field from the regular latitude-longitude grid that the OpenIFS output is on, to a spherical grid centred on the cyclone centre (the location of the maximum T42 vorticity obtained from TRACK). The spherical grid has a radius of 18 degrees and consists of 40 grid points in the radial direction and 360 grid points in the angular direction. After the meteorological fields have been interpolated onto this grid, these fields are then rotated so that all ETCs are travelling due east. Finally to obtain the ETC composite, the meteorological values on the radial grid at each offset time are averaged. Thus, the composite extra-tropical cyclone is the simple arithmetic mean of the selected ETCs.

Compared to previous studies, the composites analysed here are produced by averaging a much larger number of ETCs (e.g. > 2000). This may result in a large degree of smoothing if there is large variability between the ETCs in the selected population. Therefore, we investigated how sensitive the results of the composite mean precipitation are to the number of ETCs included in each composite by creating clusters with sub-samples of ETCs. Overall, the main conclusions are not strongly sensitive to the number of ETCs included in composites (not shown).

3.3 Cyclone Clustering

K-means clustering (Lloyd, 1982) is used to separate the ETCs into different groups with different precipitation structures. As input to the k-means clustering algorithm, we use the regridded precipitation field (convective plus large-scale precipitation) within a 12 degree radius of the ETC centre 12 hours before the time of maximum vorticity. Twelve degrees was selected as the radius as, based on plotting many individual ETCs, this provided a good balance between ensuring that all precipitation clearly related to the ETC was included and that precipitation related to another nearby ETC was excluded. It is also consistent with the radius used to attribute precipitation to ETCs in Hawcroft et al. (2012). However, to determine how sensitive the results are to this choice of radius, the clustering was repeated but with various different radii (4.5, 8, 12 and 18 degrees) of the ETC centre and these results are discussed in the Supplementary material and shown in Figure S1.

As we want to group ETCs based on their spatial distribution of precipitation, and not on the absolute precipitation values, we use quantile mapping (scikit-learn's quantile transform function, Pedregosa et al. 2011) to normalise the precipitation field

of each individual ETC to a uniform distribution. In practice, this means that for each ETC, each grid cell on the polar grid is given a value between 0 and 1 and all values (for each individual ETC) represent a uniform distribution. Quantile mapping is robust to outliers and also performs well with sparse and semi-sparse arrays.

A disadvantage of k-means clustering is that the number of clusters is not automatically selected by the algorithm and instead must be specified in advance by the user. Furthermore, it most situations there is no clear, ideal number of clusters. Usually, the optimal number of clusters is determined by trying a number of different options and calculating various measures that quantify how similar an element (i.e one ETC in our case) is to its own cluster compared to other clusters. We tested 2 to 19 clusters and for each clustering computed the silhouette score (Rousseeuw, 1987). The silhouette score ranges from -1 to +1 where large positive values indicate that the element is very well matched to its cluster. In contrast, low or negative values mean that an element is poorly matched or potentially mis-classified. The silhouette score is computed for each element (each ETC) and then the final silhouette score is the average of all elements.

Figure S2 shows the silhouette score for all three experiments as a function of cluster number. Based on these results, we use 4 clusters. A smaller number of clusters (e.g. 2) gives higher scores but little meaningful information can be obtained from only two clusters. We also select k=4 as to enable us to more easily compare the three experiments we wanted to have the same number of clusters in each experiment and for k=4, all experiments still have moderate silhouette scores and the AA experiment even exhibits a localised maximum. For k=5, and especially k=6, both the control and AA experiments see a reduction in the silhouette score although this is not the case for the SST4 simulation.

3.4 Precipitation diagnostic

To enable comparison between thousands of ETCs in each experiment, a succinct diagnostic for the ETC precipitation is required. For each ETC, we compute the average precipitation rate, P_{ave}, which is defined as

$$P_{ave} = \sum_{i=1}^{m} P_i \frac{A_i}{A_T} \qquad (1)$$

where P_i is the precipitation rate in each grid cell i and m is the number of grid cells within a given radius of the cyclone centre on the spherical grid and where P_i exceeds 1 mm / 6 hr. A_T is the total area covered by m grid cells and A_i is the area of each individual grid cell i. Hence, we average the precipitation rate but only over grid cells where precipitation is actually occurring.

4 Climatology of the three experiments

The global mean 2 m-temperature and precipitation, averaged over the 10 years of simulation, for each simulation is presented in Table 1. The control simulation has a global mean temperature of 286.7 K (13.5°C), which is similar to that of the real Earth (288 K, Hartmann (2015)), and a global mean precipitation rate of 3.18 mm day^{-1} which is larger than the real Earth due to the absence of land in these simulations. The SST4 simulation is 4.1 K warmer than the control simulation and also has a larger global mean precipitation rate (3.63 mm day^{-1}) than the control simulation. This precipitation increase equates to an

increase of 3.5% per degree of warming which is slightly larger than the most likely range of 2 - 3% found in recent climate model simulations (Douville et al., 2021). The AA simulation is 1.1 K warmer than the control simulation and when global precipitation is considered, there is a very slight decrease (0.01 mm day^{-1}) compared to the control simulation. However, when only the temperature and precipitation in the mid-latitudes (25 - 70°N) are considered, the AA simulation warms by 1.6 K and the precipitation increases by 0.06 mm day^{-1}, equivalent to an increase of 1.54% per degree of warming.

Basic statistics of the characteristics of the objectively identified ETCs are shown in Table 2. There are 578 fewer ETCs identified in the SST4 simulation compared to the control simulation, however the decrease is not statistically significant when a t-test is performed on the yearly totals (N=10) assuming unequal variance. In contrast, 440 more ETCs are identified in the AA simulation than in the control and this difference is statistically significant. Notably, there is more year-to-year variation in the number of ETCs in the SST4 simulation compared to both the control and AA simulations (Table 2).

The mean and median values of the maximum relative vorticity of the ETCs in the control and SST4 simulations are very similar (Table 2). The full distributions (Fig. 2a) are also very similar and do not differ statistically when a two-sided t-test is performed. However, the SST4 simulation has a broader distribution with both more weak and more strong ETCs. In the SST4 simulation 12.1% of ETCs have a maximum vorticity exceeding $10 \times 10^{-5} s^{-1}$ whereas only 10.3% of ETCs exceed this threshold in the control simulation. The mean and median maximum relative vorticity of all ETCs in the AA simulation is smaller than in the control simulation (Table 2) which is also evident in the full distribution (Fig. 2a). A one-sided t-test shows that the maximum vorticity values in the AA experiment are statistically significantly weaker than in the control simulation. This is consistent with the fewer very strong ETCs in the AA simulation compared to both the control and SST4 simulations.

The genesis and lysis latitudes of the ETCs in each simulation are also considered and in all simulations exhibit roughly Gaussian distributions. The genesis and lysis latitudes of ETCs move polewards in SST4 compared to the control whereas the opposite behaviour occurs in the AA simulation (Table 2 and Fig. 2b,d).

Lastly as the focus on this study is on ETC related precipitation, we also considered the distributions of the ETC averaged precipitation in each simulation (Fig. 2c). In all experiments, there is a localised peak for very weak (1.25 - 1.5 mm / 6 hr) precipitation amounts. This is partly because of the 1 mm / 6 hr threshold used in the precipitation diagnostic (Equation 1). This localised peak is more pronounced in the AA experiment as there are more ETCs with weak precipitation compared to the other two experiments. The control simulation has more ETCs with weak to moderate precipitation (2 - 3 mm / 6 hr) than either the SST4 or AA simulations, potentially as, on average, the control is the coldest simulation. The SST4 simulation has many more ETCs with precipitation amounts exceeding 4 mm / 6 hr than in either the control or AA simulations, which show very similar distributions for heavier precipitation amounts. A t-test confirms that there is no significant difference between the control and AA simulation in terms of ETC related precipitation. In contrast, t-tests show that ETCs in the SST4 experiment have statistically significantly more precipitation associated with them than ETCs in the control simulation.

The distribution of the maximum vorticity of ETCs differs between the three simulations. Therefore, an Analysis of Co-variance (ANCOVA) is applied here to determine if the ETC related precipitation differs in the different experiments, after controlling for a covariate, which in this case is the maximum vorticity of the ETC. This allows us to test the null hypothesis, which is that ETCs with the same intensity (measured in terms of the relative vorticity) have the same amount of precipitation

associated with them in each experiment. This analysis shows that ETCs in the SST4 simulation have more precipitation than those in the control simulation even after accounting for the differences in ETC maximum vorticity. This is as expected, given that there was no significant difference between the maximum vorticity distributions yet notable differences in the precipita-

255 tion. Of more interest is to apply ANCOVA to the control and AA simulations as the AA simulation has weaker cyclones yet the same amount of ETC related precipitation. After controlling for the differences in ETC maximum vorticity, we find that the ETCs in the AA simulation have statistically significantly different amounts of precipitation associated with them i.e. on average, ETCs with the same intensity in the two simulations have different amounts of precipitation associated with them.

5 The relationship between precipitation and cyclone intensity

260 The relationship (slope of the linear regression) and correlation between the maximum vorticity and ETC-related precipitation at different offset times relative to the maximum vorticity were considered (Table 3). In all experiments, large correlations and positive slopes occur between maximum intensity and precipitation 24, 12 and 0 hours before the time of maximum intensity. The smallest correlations and weakest slopes occur between maximum vorticity and precipitation 24 hours after the time of maximum vorticity. Here we focus on the relationship between maximum vorticity and precipitation 12 hours before the time

265 of maximum vorticity, as shown in Figure 3, as this is when the strongest correlation occurs. Similar figures to Figure 3 except for precipitation 24 and 0 hours before the time of maximum vorticity are shown in the Supplementary material (Figs. S3 and S4).

Both the SST4 and the AA simulations have steeper slopes and thus a stronger linear relationship between maximum vorticity and precipitation than the control simulation. To determine if these slopes are statistically different, boot-strapping is applied.

270 Bootstrapping quantifies how much random variation in the slope and intercept values of the fitted linear model are due to small changes in the input data. For each experiment, we re-sample the data 5000 times using a sample size equal to that of each original data set. Thus, some pairs of data are represented multiple times in any one individual bootstrap sample while other pairs are not selected at all. For each re-sample, a linear regression is made and the slope and intercept of this model calculated. For the control simulation the estimated slopes vary from 0.261 - 0.287 (mm / 6 hr) s, for the SST4 simulation the

275 values are 0.313 - 0.348 (mm / 6 hr) s, and for the AA simulation the estimated slopes range from 0.298 - 0.326 ((mm / 6 hr) s. The resulting distributions of the computed slopes (Figure S5 in Supplementary material) for each experiment are then compared using a student's t-test and we find that the slopes are all statistically significantly different at the 99% level. Thus, we can conclude that there is a stronger relationship between maximum vorticity and precipitation in the SST4 experiment than in both the control or the AA experiment and also that the AA experiment has a stronger relation that the control. This means

280 that for the same increase in maximum vorticity, precipitation increases more in the SST4 and AA experiments compared to the control. Since the SST4 and AA experiments are both warmer than the control experiment this is to be expected based on the Clausius-Clapeyron relationship between temperature and vapour pressure. However, this also indicates that there is no (or weak) feedback onto the vorticity of the ETC from the enhanced precipitation via a diabatically produced low-level PV anomaly; if this was the case, similar slopes would be found in all experiments.

285   The most spread and thus smallest correlation coefficient (0.574) occurs in the SST4 simulation suggesting that in this simulation, the dynamical intensity of the cyclone has less control on the amount of precipitation that in the other simulations. This is likely due to the warmer atmosphere (Table 1) and more diabatic heating in this case than the control or AA simulations. The largest correlation coefficient and hence least spread occurs in the AA simulation. However, in all three simulations the correlation coefficients are not exceptionally large and we hypothesise that a large degree of the spread is caused by different

290   types of ETCs having different relationships between their intensity and their precipitation.

6   Different types of ETCs according to their precipitation patterns

Figures 4a-d show the composite mean total precipitation for each of the four clusters identified by the k-means clustering in the control simulation 12 hours before the time of maximum intensity (additional times are shown in Figure S6). The precipitation pattern differs between all four mean ETCs meaning that the k-means clustering has successfully separated the ETCs into

295   different classes.

6.1   ETC composites in the control simulation

The composite mean ETC in Fig. 4a has a large area of very heavy precipitation, exceeding 7 mm / 6 hr. The position of the warm and cold fronts, and the warm sector, is evident in the 850-hPa potential temperature (Fig. 4a) and total column water vapour (TCWV, Fig. 5a). The precipitation is heaviest near where the warm and cold fronts meet but also extends along the

300   cold front and parts of the warm sector. The convective precipitation (Fig. 5a) is moderate in intensity and only located on the poleward parts of the cold front. Hence, this composite mean is subsequently referred to as the "cold front" ETC. This cold front ETC has a very narrow warm sector which is immediately equatorward of the ETC centre. Since this ETC is meridionally extended yet zonally confined it exhibits similarities with the Norwegian cyclone model (Bjerknes, 1919). This cold front ETC is also located directly in the left-hand exit region of a strong (>50 ms^{-1}) jet streak where strong forcing for ascent due to

305   positive vorticity advection can be expected. A strong upper-level PV anomaly visible in the 315K isentropic potential vorticity (IPV, Fig. 6a) is also present immediately upstream of the ETC centre. Consequently, this mean ETC is a strong system with a minimum MSLP of 978 hPa (Fig. 6a). The 315K IPV pattern also shows this ETC is wrapped up in a cyclonic manner.

The precipitation pattern associated with the second identified ETC is of moderate intensity (up to 3.5 mm / 6 hr) and is mainly associated with the warm front, a bent-back warm front (which hooks around the poleward and upstream side of the

310   ETC centre) and in the warm sector (Fig. 4b). Thus, this composite is here-in-after referred to as the "warm front ETC". The warm front ETC has a broad warm sector, evident in both the 850-hPa potential temperature (Fig. 4b) and TCWV (Fig. 5b), which is shifted well downstream of the ETC centre. The strongest ascent (Fig. 6b) is co-located with the heaviest precipitation on the warm front. Very little (< 1 mm (6 hr)$^{-1}$) convective precipitation is associated with this mean ETC (Fig. 5b). The 850-hPa potential temperature shows that both the warm and cold front have similar temperature gradients associated with

315   them. The zonally broad nature of this mean ETC suggests that it resembles the Shapiro-Keyser conceptual model (Shapiro and Keyser, 1990). Similar to the cold front ETC, the warm front ETC is also located on the poleward side of a jet streak.

However, this ETC is not directly in the left-hand exit region, but is located 10 degrees (on the rotated polar grid) poleward of the 45 ms^{-1} jet streak (Fig. 6b), which likely explains the weaker vertical motion and precipitation associated with this ETC. This ETC also has strong IPV anomaly at upper levels and is also shows signs of cyclonic wave breaking.

320   The precipitation associated with the third type of ETC identified by the k-means clustering is shown in Figure 4c. This ETC is also located in the left-hand exit region of a jet streak but the jet streak is weaker than those associated with either the warm front or cold front ETC (Fig. 6c). The precipitation associated with this ETC has a small spatial extent and is mainly focused on the ETC centre. Therefore, this composite mean is subsequently referred to as the "centre" ETC. Despite the weaker jet streak, and high minimum MSLP (991 hPa) the centre ETC has heavier precipitation and stronger ascent than the warm front ETC.

325   This is likely explained by the moister air advected towards the centre of this ETC: the TCWV values reach to 13 g kg^{-1} in the ETC centre in this small cyclone but only to 10 g kg^{-1} in the warm front ETC. In agreement with the increased moisture, this ETC has more convective precipitation associated with it than the warm front ETC. This ETC also differs from the warm and cold front ETCs in that it does not have a large low pressure centre and only a small-scale closed circulation. Furthermore, at upper levels this ETC has a weaker IPV anomaly and is less cyclonically wrapped up than the other two ETCs, remaining

330   more of an open wave at upper levels. This weaker upper level forcing may explain why the MSLP is not very low.

     The precipitation pattern of the fourth and last ETC type is shown in Figure 4d. This ETC differs considerably from all other ETCs. Firstly, it is much weaker in terms of vertical motion (Fig. 6d) than all other ETCs, although a closed circulation is evident with a minimum MSLP of 991 hPa (which is almost the same minimum MSLP as seen in the centre ETC). Secondly, this weak ETC is not located in the jet exit but rather is located far poleward of the jet stream and does not have a pronounced

335   upper level IPV anomaly upstream of the ETC centre. Lastly, this ETC is located in a cold and dry air mass; the TCWV values near the ETC centre are around 7 g kg^{-1} (Fig. 5d) and the 850-hPa temperature values are 278K (Fig. 4d). The total and convective precipitation associated with this ETC are also much weaker than in all other mean ETC. Therefore, this composite mean is subsequently referred to as the "weak" ETC.

     So far, only the mean structure of each cluster has been presented. Figures 7, 8, and 9 show the distributions of the ETC

340   related precipitation, maximum vorticity and the latitude of the maximum vorticity for each cluster. The shapes of the precipitation, maximum vorticity and latitude of maximum vorticity distributions are similar for the cold front, warm front and centre ETC however the weak ETCs have very different shaped distributions, particularly for the latitude of maximum vorticity. The distributions for each cluster within the control simulation can be compared to each other using Student's t-test to determine how different the clusters are and also to explain the differences in the mean ETC structures.

345   When the full distributions for each cluster in the control simulation are considered (Fig. 7a, d, g, k), the cold front ETCs have statistically significantly more precipitation associated with them than the ETCs in the other three clusters, which is in agreement with the mean values presented in Figure 4. The cold front ETCs also have statistically significantly larger values of maximum vorticity compared to all other clusters (Fig. 8a, d, g, k) and also reach their maximum vorticity values further south (mean latitude of 44.4°N) than ETCs in the other three clusters.

350   The centre ETCs in the control simulation have statistically significantly more precipitation associated with them than the warm front ETCs despite that the warm front ETCs have stronger maximum vorticity values (the difference is statistically

significant). The mean latitude that ETCs in the centre ETC cluster reach their maximum vorticity at is 45.1°N compared to 47.4°N for ETCs in the warm front cluster (Fig. 9). The distributions of latitude of the maximum vorticity also differ in a statistically significant way. The weak ETCs in the control simulation have the smallest maximum vorticities associated with
355 them but also occur at much higher latitudes than the other types of ETC.

6.2 ETC clusters in the SST4 and AA simulations

Figures 4e-h and i-l show the precipitation patterns, MSLP and 850-hPa potential temperature for the four composite mean ETCs in the SST4 and AA simulations (additional times for the SST and AA experiments are shown in Figure S7 and S8 respectively). The main result is that in all three experiments, very similar types of ETCs in terms of their precipitation patterns
360 occur; the cold-front, warm-front, small and weak cyclone identified in the control simulations also occur in the SST4 and AA simulations. Furthermore, the dynamical structure and location relative to the jet streak is very similar for all clusters in the SST4 and AA experiments compared to the corresponding cluster in the control simulation. However, some differences do exist, particularly in terms of the absolute values of thermodynamic variables.

The mean ETCs in the SST4 experiment all have heavier total precipitation and convective precipitation than in the control
365 simulation although the spatial patterns are very similar. Likewise, the mean composite ETCs in the SST4 experiment all have much higher values of TCWV and 850-hPa potential temperature associated with them. This is consistent with an overall warmer and thus moister environment. Related to this, the SST4 composite means have lower IPV values on the 315K isentrope, caused by this isentrope being lower in the troposphere in the warmer simulation. The minimum MSLP is 1 - 3 hPa deeper in the SST4 mean ETCs compared to their related clusters in the control simulation. Interestingly, the vertical motion at 700
370 hPa is almost identical in the corresponding composites in the control and SST4 simulations, indicating that the large increase in precipitation is not related to changes in dry dynamics. The only discernible difference in the ETC structure occurs for the warm front ETC. In the SST4 simulation this is associated with a weaker jet streak compared to the control.

Now the distributions of precipitation, maximum vorticity and latitude of maximum vorticity for each cluster in the SST4 simulation are compared to the corresponding cluster in the control simulation. A summary of the statistically significant dif-
375 ferences is presented in Figure 10. When the distributions of ETC precipitation for each cluster in the SST4 simulation are compared to the corresponding cluster in the control simulation, one-sided t-tests show that all clusters in the SST4 experiment have statistically significantly more precipitation associated with them (Figs. 7, 10). The cold front ETCs in the SST4 simulation have statistically significantly larger values of maximum vorticity compared to the corresponding cluster in the control simulation (Figs. 8, 10). However, when the warm front and centre ETC clusters are considered, there is no statistically sig-
380 nificant difference between the distributions of maximum vorticity between the SST and control simulations. Furthermore, the weak ETC cluster has statistically significantly smaller values of maximum vorticity compared to the corresponding cluster in the control. This means that how the maximum vorticity of ETCs responds to uniform warming depends on the type of ETC. This result is consistent with the result presented in section 4 - that uniform warming does not change the maximum vorticity of ETCs - but also indicates that looking at all ETCs together can mask notable changes. The cold front, warm front and centre
385 ETCs occur at higher latitudes in the SST4 simulation in comparison to their counterparts in the control simulation (Figs. 9,10).

However, in the SST4 experiment, the weak ETCs occur at slightly lower latitudes (mean latitude of 60.8°N) than the weak ETCs in the control simulation.

We now compare the cluster means in the AA simulation to the corresponding clusters in the control simulation. All ETCs have significantly more precipitation associated with then in the AA simulation (Figs. 4). However, the increases are relatively

390 small except for the warm front ETC, which has an increase of almost 1 mm $(6 \text{ hr})^{-1}$ in the precipitation rate on the bent-back warm front. In addition, although the MSLP patterns are very similar between the AA and control composite mean ETCs, the minimum MSLP is 2 - 4 hPa higher in the AA simulation than in the control. The jet structure, 700-hPa ascent, and upper level IPV fields are also very similar between the AA ETC cluster means and those in the control.

When the ETC precipitation distributions for each cluster in the AA simulation are compared to the corresponding cluster

395 in the control simulation, we find that the ETCs in the cold front, warm front and centre ETCs clusters have more precipitation associated with them in the AA simulation than in the control (summary shown in Fig. 10. In contrast, the precipitation associated with weak ETC cluster has no significant difference between the AA and control simulation. The cold front, small, and weak ETC clusters have statistically significantly weaker maximum vorticity values in the AA simulation compared to in the control simulation (Figs. 8, 10). The maximum vorticity of the ETCs in the warm front cluster does not differ between the

400 AA and the control simulation. All clusters have their latitude of maximum vorticity more equatorward in the AA simulation compared to the control (Fig. 9). This result is statistically significant for all clusters (Fig. 10) and consistent with the changes in genesis and lysis latitude presented in Figure 2.

6.3 Frequency of occurrence of the different ETCs

To help answer the question of whether different types of ETCs are more or less common in the different climates, the number

405 of ETCs in each cluster for each experiment and the relative occurrence of the 4 types of ETCs is shown in Figure 11. In the control simulation the absolute number of ETCs in the warm front, cold front and the small cyclones is very similar. However, there are slightly more ETCs in the weak cyclone cluster. In the SST4 simulation, again the weak cyclone cluster has the most ETCs. The cold front ETC cluster is the second most common but closely followed by both the warm front and small cyclones. In the AA simulation the number of weak ETCs in much larger than in the other three ETC types and also much

410 larger than the absolute number and relative occurrence of weak ETCs in the control or SST4 simulation. This indicates that Arctic amplification and the associated decrease in the large-scale low-level temperature gradient and increase in high latitude temperatures leads to many more weak ETCs developing.

7 Effect of ETC type of the relationship between precipitation and cyclone intensity.

Figure 12 shows the relationship between maximum vorticity and total precipitation 12 hours before the time of maximum

415 intensity for each cluster in each experiment. In all experiments, the largest correlation and strongest relationship occurs for the warm front cyclone cluster (Fig. 12d, e, f). These are not the strongest ETCs in terms of maximum vorticity, minimum MSLP or ascent. Furthermore, the warm front ETCs are typically located further poleward of the jet streak and also at slightly higher

latitudes than the cold front cyclones. These warm front cyclones also have relatively little convective precipitation associated with them which likely explains the stronger relationship between maximum vorticity and total precipitation.

420 Moderately strong and still positive relationships exist between precipitation and vorticity for the cold front cluster (Fig. 12a, b, c), particularly in the SST4 experiment. This is the cluster with the heaviest precipitation and strongest maximum vorticity values. The cold front ETCs also reach their maximum intensity at relatively low latitudes and thus develop in warmer and moist environments. Therefore the precipitation in these ETCs is not limited by moisture availability and this is likely why the maximum vorticity is a relatively good predictor for the amount of precipitation. Furthermore, these ETCs have more

425 convective precipitation associated with them than the warm front cyclones which may be one reason why the relationship between maximum vorticity and total precipitation is weaker.

In contrast, there is not a strong linear relationship between the maximum vorticity and the total amount of precipitation in the centre ETC cluster and a poor (r < 0.15) correlation (Fig. 12g, h, i). This result is applicable for all experiments. There are ETCs included in the centre ETC cluster which have small values of maximum vorticity yet moderate to large amounts of

430 precipitation associated with them. It is likely that these ETCs are strongly convective and hence the precipitation amount is not influenced by the large-scale ascent or the strength of the circulation.

The weak ETCs also lack a strong relationship between maximum vorticity and precipitation and this is a robust result across all experiments. This is very likely explained by the high latitude of these ETCs and the limited about of moisture available in the locations they develop in and move through.

435 **8 Conclusions**

In this study, we investigate the relationship between the maximum intensity of extra-tropical cyclones and their precipitation, how this may change in the future, and also how it depends on the type of ETC. Three aquaplanet simulations were performed with the state-of-the-art numerical prediction model, OpenIFS, differing only in terms of their prescribed SST distributions. A control simulation, a uniform warming and a polar amplification experiment were conducted.

440 First, the impact of uniform warming and polar amplification on the cyclone statistics was investigated. Uniform warming resulted in an increase in ETC precipitation, a small poleward shift in the storm track, no statistically significant change to the mean or medium maximum vorticity but more extreme ETCs in terms of their maximum vorticity. In contrast, polar amplification lead to no change in ETC precipitation, weaker ETCs in terms of their maximum vorticity, and a small equatorward shift of the storm track. These results agree with previous results from both idealised modelling experiments and fully coupled

445 realistic climate models (e.g. Yettella and Kay, 2017; Priestley and Catto, 2022) which gives confidence in the relevance and robustness of our idealised simulations.

In all three experiments, there is a positive correlation between the ETC maximum 850-hPa vorticity and average precipitation, which is in agreement with previous studies (e.g. Pfahl and Sprenger, 2016). The strongest relationship (slope) is in the uniform warming (SST4) experiment and the weakest in the control. Thus, the same absolute increase in cyclone strength in

450 SST4 corresponds to a larger increase in ETC-related precipitation than in the control simulation. SST4 is the warmest and

wettest simulation globally which likely explains the strongest slope, especially when the results of Yettella and Kay (2017), who showed most of the increase in ETC precipitation is due to thermodynamic aspects, are considered. Theoretically, heavy precipitation causes strong diabatic heating which, in turn, could increase the intensity of the ETC via the production of a low-level positive vorticity anomaly. However, in our warmer experiments, precipitation strongly increases but there is not any

455　large increase in the intensity of ETCs i.e. the slope is larger in SST4 than in the control. This implies that the increased diabatic heating does not feedback strongly onto the intensity of the ETCs in these experiments. The horizontal resolution of these simulations is relatively coarse at 80 km, and if similar experiments were performed with a much higher resolution model, the amount of diabatic heating and the strength of the low-level PV anomaly would very likely increase; this was recently shown to happen by Choudhary and Voigt (2022). Potentially, the diabatic feedback may become more visible at high resolution, in

460　which case, we would expect that the slopes of the linear regression lines between maximum vorticity and precipitation would be similar - albeit shifted to larger values in the warmer simulations. However, whether a feedback occurs may depend on the type of cyclone. In the one case study that Choudhary and Voigt (2022) considered, the stronger diabatic heating and potential vorticity at higher resolution did not result in a lower MSLP as the cyclone was strongly dominated by thermal advection and diabatic heating played a secondary role in its intensification.

465　The variability (spread) in the relationship between precipitation and ETC intensity also varies between the experiments. The smallest correlation coefficient (r) is found in the SST4 experiment suggesting there is larger variability in ETC-related precipitation in the SST4 experiment than in either the control or polar amplification experiment. All experiments do show considerable spread (the correlation coefficients range between 0.574 and 0.635) which suggests that not all ETCs have a strong connection between ETC intensity and precipitation. This large spread motivated us to cluster the ETCs into 4 groups

470　using k-means clustering and investigate how the relationship between precipitation intensity and cyclone intensity depends on cyclone type.

The clustering proved to be successful. Four distinct and physically realistic mean cyclones were identified by compositing all ETCs allocated to each cluster together. Each cluster (mean composite ETC) could be labelled based on their precipitation patterns: a cyclone where most precipitation was associated with the cold front (cold front ETC), a cyclone where most pre-

475　cipitation was associated with the warm front (warm front ETC), a small-scale cyclone with most precipitation located near the cyclone centre (centre ETC) and a small-scale, high latitude cyclone with weak precipitation again focused on the cyclone centre (weak ETC).

The first notable result from the clustering is that the same four mean ETCs are identified in all three experiments despite the clustering being done independently for each simulation. This suggests that neither uniform warming nor polar amplification

480　will lead to any notable changes in the spatial patterns of precipitation associated with ETCs. The second main result of the clustering is that the absolute number and relative occurrence of the weak ETC, which was found to develop in cold air masses far poleward of the jet stream, increases considerably with polar amplification, despite the large-scale meridional temperature gradient decreasing. We hypothesise that this is because the polar regions are much warmer, making diabatic heating and convection more possible, which then may organise into the weak ETCs. This indicates that high latitude cyclones may become

485　more common in the future.

The third main result from the ETC clustering is that the relationship between maximum vorticity and precipitation depends strongly on the type of ETC. The strongest relationship occurs for the warm front ETCs and this result is robust across all three experiments. These ETCs are moderately strong, resemble the Norwegian cyclone model, and have little convective precipitation associated with them. The lack of convective precipitation suggests that the precipitation is driven by large-

490 scale forcing which may explain the strong relationship between the precipitation and maximum vorticity. However, another hypothesis is that in these ETCs, heavy precipitation on the warm front causes a low-level positive PV anomaly to develop close to the centre of the ETC, which is in a location where it can interact and feedback onto the vorticity of the ETC. A strong correlation is also found between maximum voricity and precipitation for the cold front ETCs, but this is slightly weaker, and has more spread, than what was found for the warm front ETCs. The cold front ETCs are, on average, the strongest ETCs in

495 terms of vorticity, ascent and precipitation.

The weak ETC has a notably smaller correlation between ETC precipitation and maximum vorticity in all experiments (correlation coefficients range from 0.241 to 0.298). These ETCs occur at high latitudes and therefore we conclude that the ETC precipitation is limited by the lack of moisture and hence that the dynamic intensity of the ETC has little control on the ETC precipitation.

500 The weakest of all correlations between the ETC precipitation and vorticity occurs for the cyclone centre ETC (correlation coefficients range from 0.098 to 0.190). Binder et al. (2016) classified cyclones based on their deepening rate and warm conveyor belt intensity and one of their subsets, C2b, has a strong warm conveyor belt and low-level PV anomaly but does not deepen rapidly, which Binder et al. (2016) attribute to the lack of upper level forcing. This C2b composite cyclone also has precipitation located over a relatively small area near the cyclone centre and thus resembles our weak cyclone composite.

505 Therefore, we hypothesise that the poor correlation we find between ETC precipitation and vorticity in the cyclone centre cyclone is due to the lack of strong upper level forcing for these ETCs, as suggested by Binder et al. (2016).

The final notable result from the clustering is that how the maximum vorticity of the ETCs response to uniform warming depends on the type of ETC. The cold front ETC sees an increase in its maximum vorticity with uniform warming whereas both the warm front and cyclone centre ETCs show no change in the maximum vorticity and the maximum vorticity of the

510 weak ETC decreases. Hence this is consistent with the overall picture, when all ETCs are considered together that there are no changes in ETC intensity, however it does suggest that the dynamical intensity of certain types of ETCs may respond more to climate change than others. This result is also in agreement with previous studies (e.g. Priestley and Catto, 2022) which show that extremes respond differently to warming as the cold front ETC includes the strongest ETCs.

Our study is unique in some aspects. First, previous studies have tended to relate ETC precipitation to the ETC winds

515 whereas we use the maximum vorticity as identified by TRACK. This approach was selected as maximum vorticity is easily available from climate model simulations and is often the variable that is used when the question of how will the intensity of ETCs change in the future is addressed. Our study also differs from many previous studies in that we consider ETCs of all strengths and not just the extremes in terms of either their maximum vorticity (as was done by Sinclair et al. (2020)) or precipitation. This does make a difference to how future changes are seen (Priestley and Catto, 2022). However, our study does

520 highlight that despite small changes in the strength of the cyclones, the precipitation increases are large, indicating potential

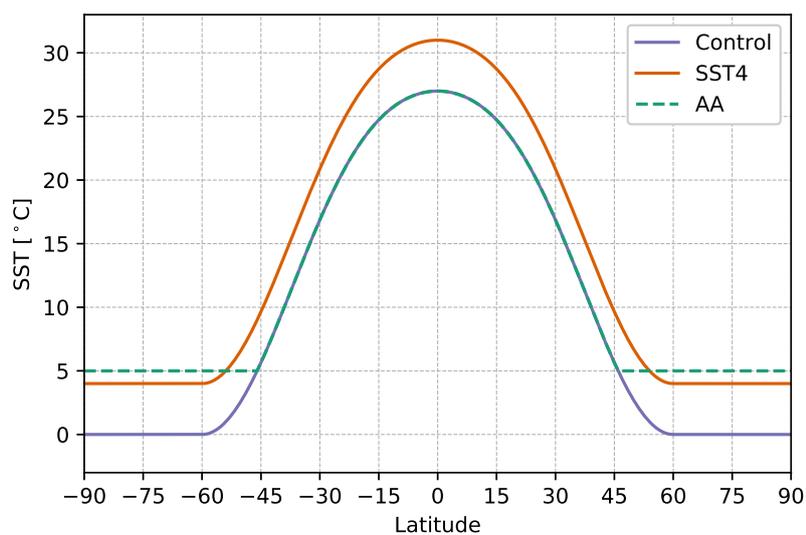future increases in flooding associated with cyclones.

Figure 1. Sea surface temperature distribution as a function of latitude for the three experiments. The control simulation is shown in purple which has the QObs SST distribution, SST4 (orange) is uniform warming and AA (dashed green) is warmed poles.
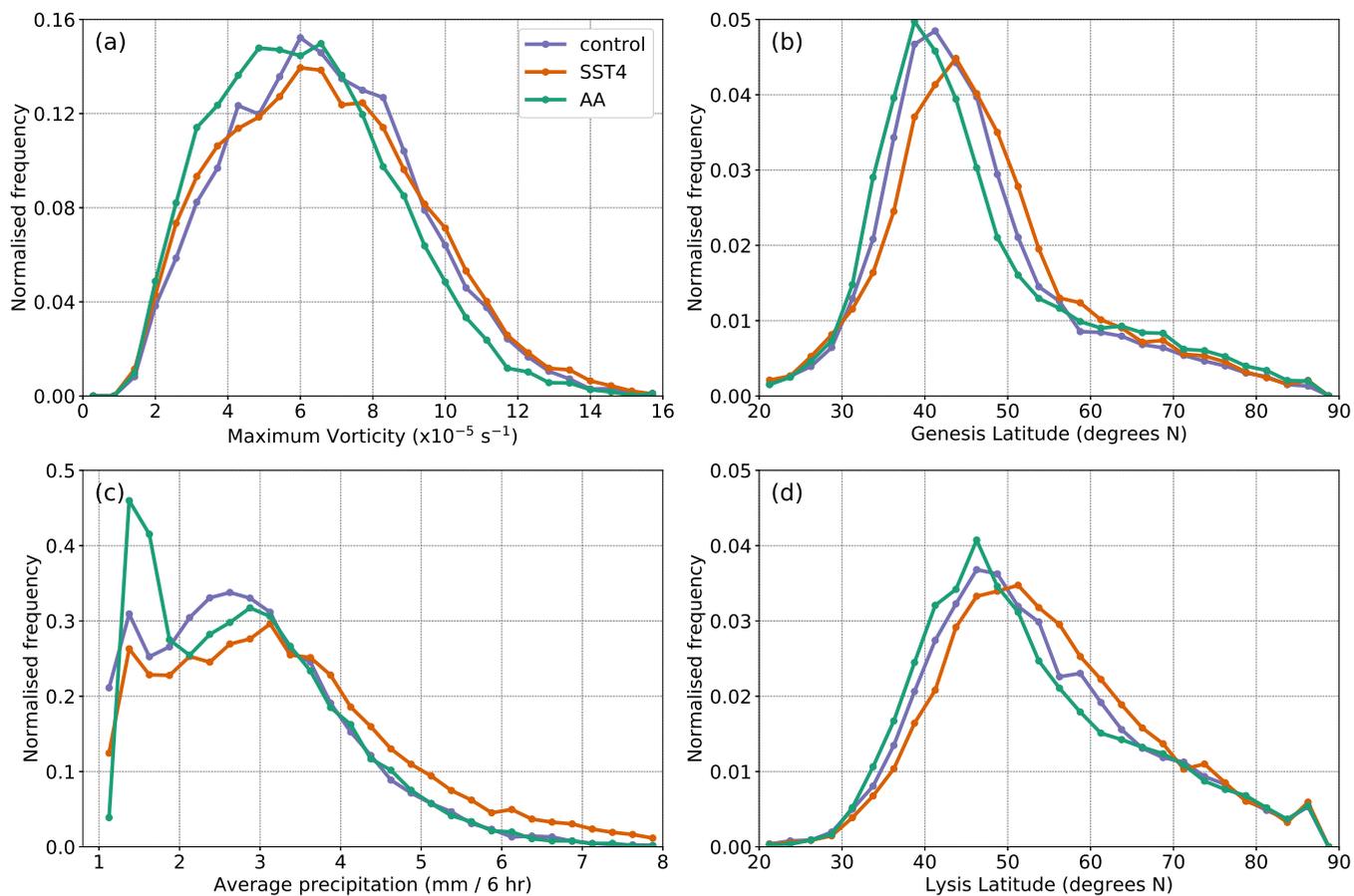
Figure 2. Probability density distributions of the (a) maximum relative vorticity (T42 values), (b) genesis latitude, (c) average ETC precipitation 12 hours before the time of maximum intensity and (d) lysis latitude for each experiment. Cyclones are only included if they exist 24 hours before the time of maximum vorticity and reach their maximum vorticity poleward of $30°$N.
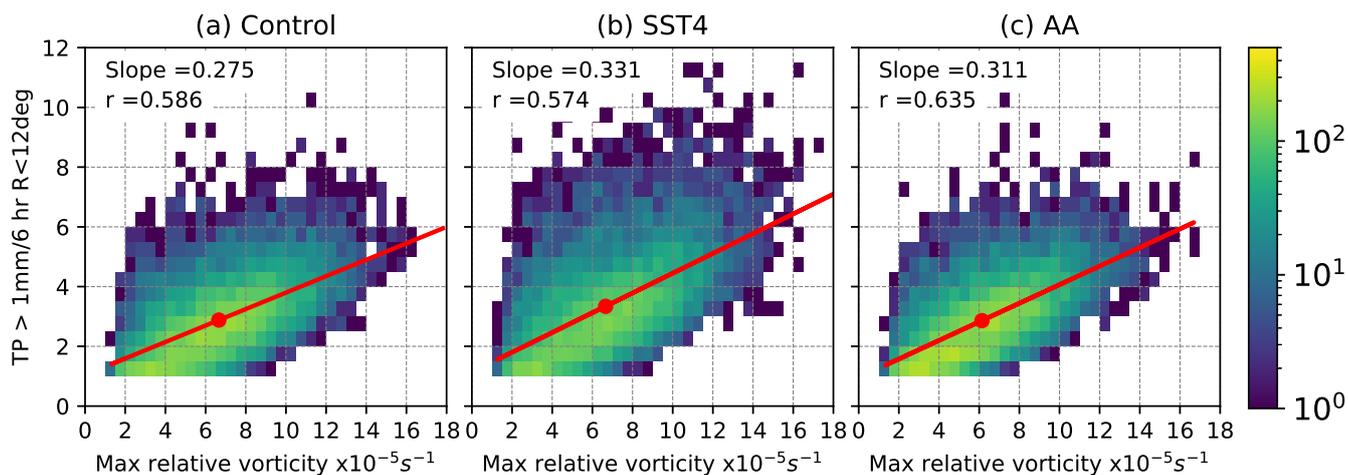
Figure 3. Two-dimensional histograms showing the relation between maximum relative vorticity (T42 values) and ETC-related precipitation 12 hours before the time of maximum relative vorticity. Precipitation is the area average, averaged over all points within a 12 degree radius of the ETC centre where the rain rate exceeds 1 mm / 6 hr. Only ETCs which exist at -24 hr and have their maximum vorticity north of $30°N$ are included. The slope values have units of (mm / 6 hr) s.
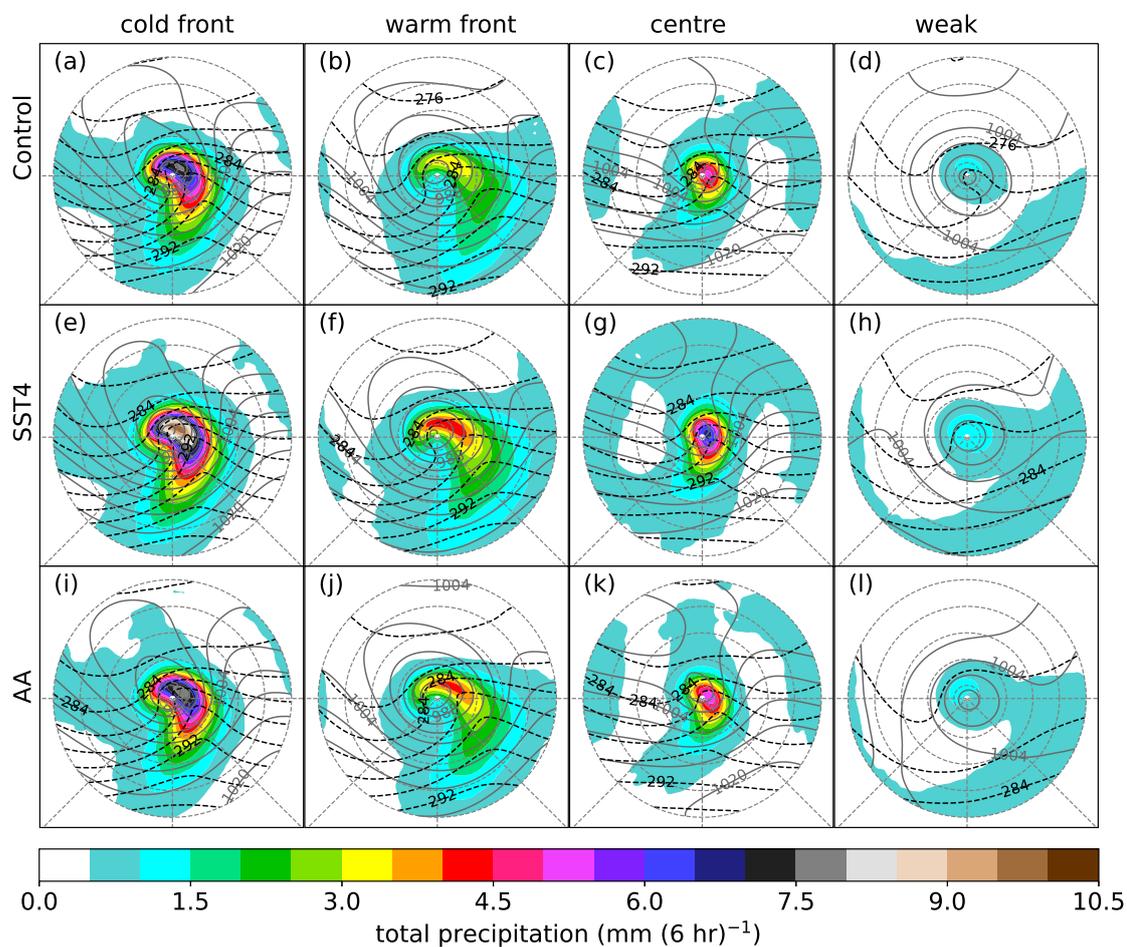
Figure 4. Composite mean of the total precipitation (shading, mm / 6 hr), mean sea level pressure (grey contours, every 4 hPa) and the 850-hPa potential temperature (dashed contours, every 2 K) 12 hours before the time of the maximum vorticity. Different columns show different clusters and different rows show different experiments.
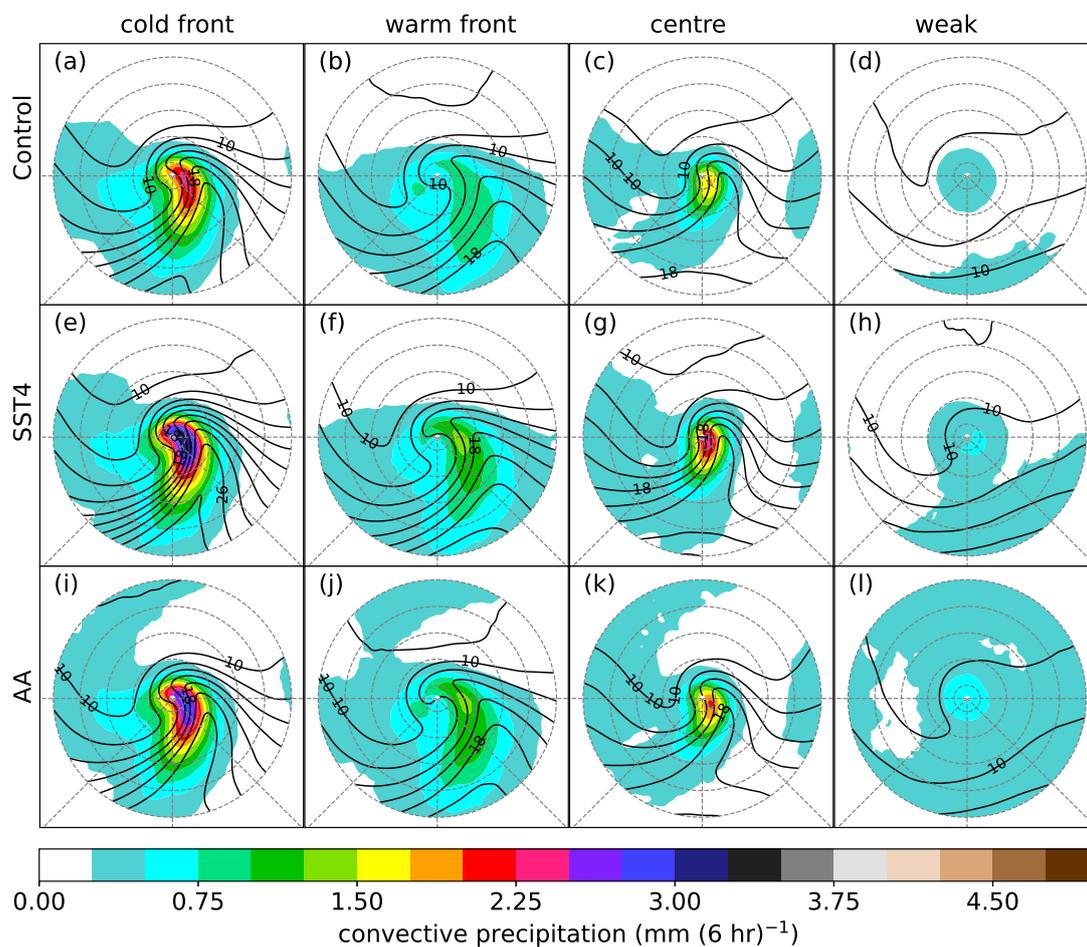
**Figure 5.** Composite mean of the convective precipitation (shading, mm / 6 hr) and the total column water vapour (black contours, every 2 g kg^{-1}) 12 hours before the time of the maximum vorticity. Different columns show different clusters and different rows show different experiments.
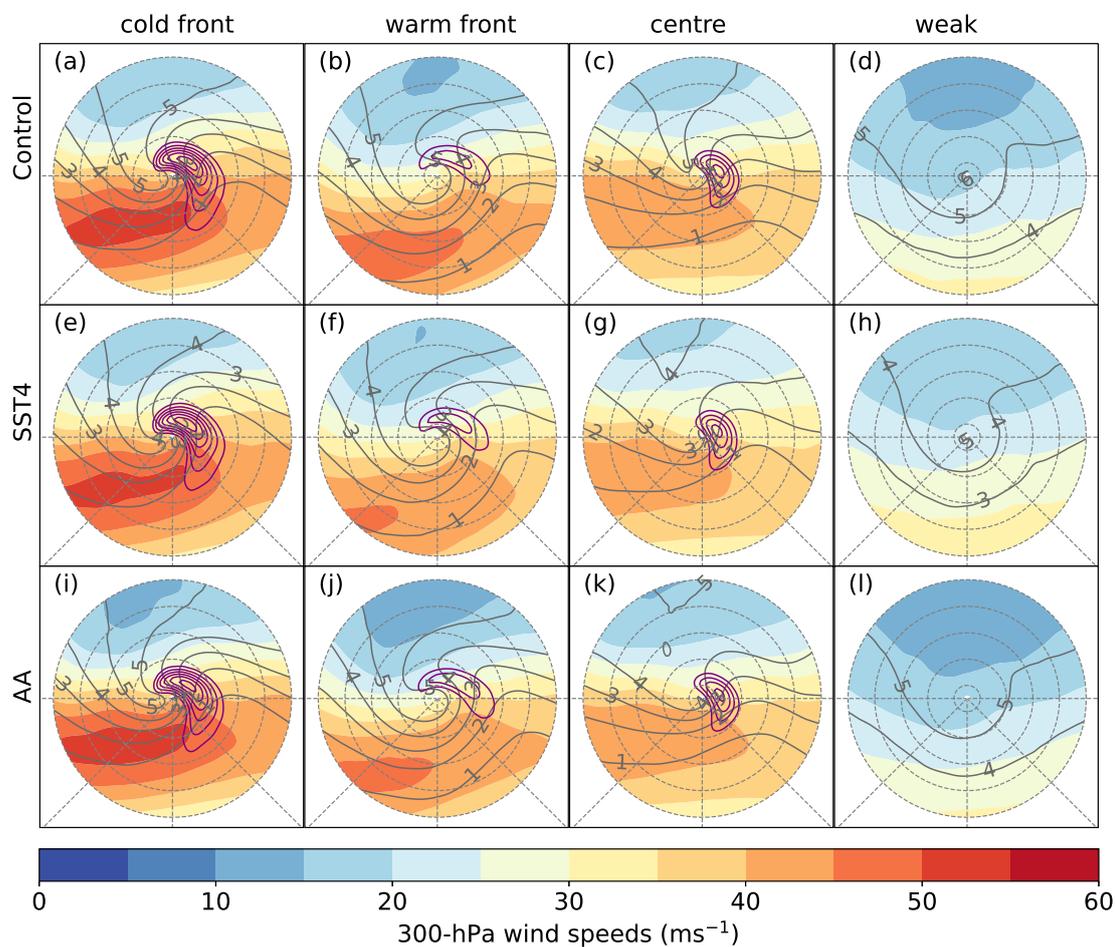
Figure 6. Composite mean of the 300-hPa wind speed (shading, m s^{-1}), potential vorticity on the 315K surface (grey contours, every 1 PVU) and the 700-hPa vertical velocity (solid purple contours, only ascent shown - (first contour is -0.2 Pa s^{-1}, contour interval of 0.1 Pa s^{-1}) 12 hours before the time of the maximum vorticity. Different columns show different clusters and different rows show different experiments.
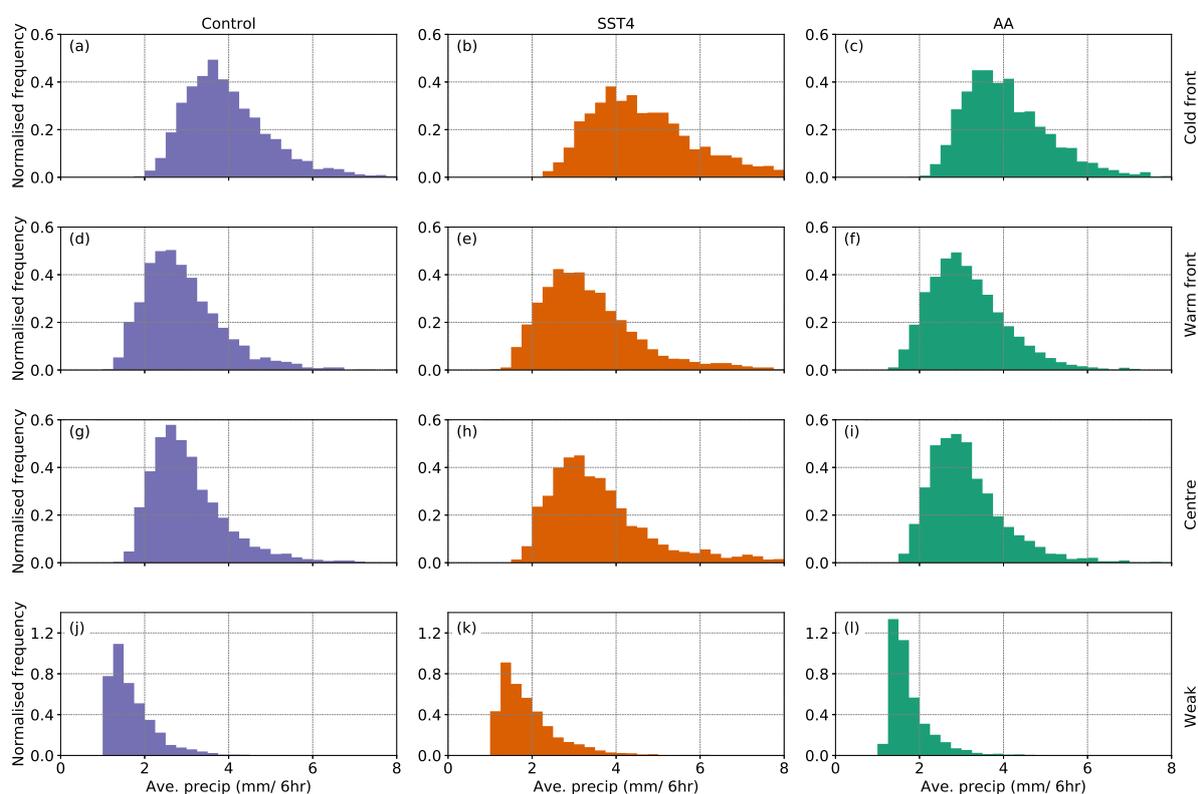
Figure 7. Probability density distributions of the average ETC precipitation 12 hours before the time of maximum intensity for each cluster (different rows) and each experiment (different columns). Cyclones are only included if they exist 24 hours before the time of maximum vorticity and reach their maximum vorticity poleward of $30°$N.
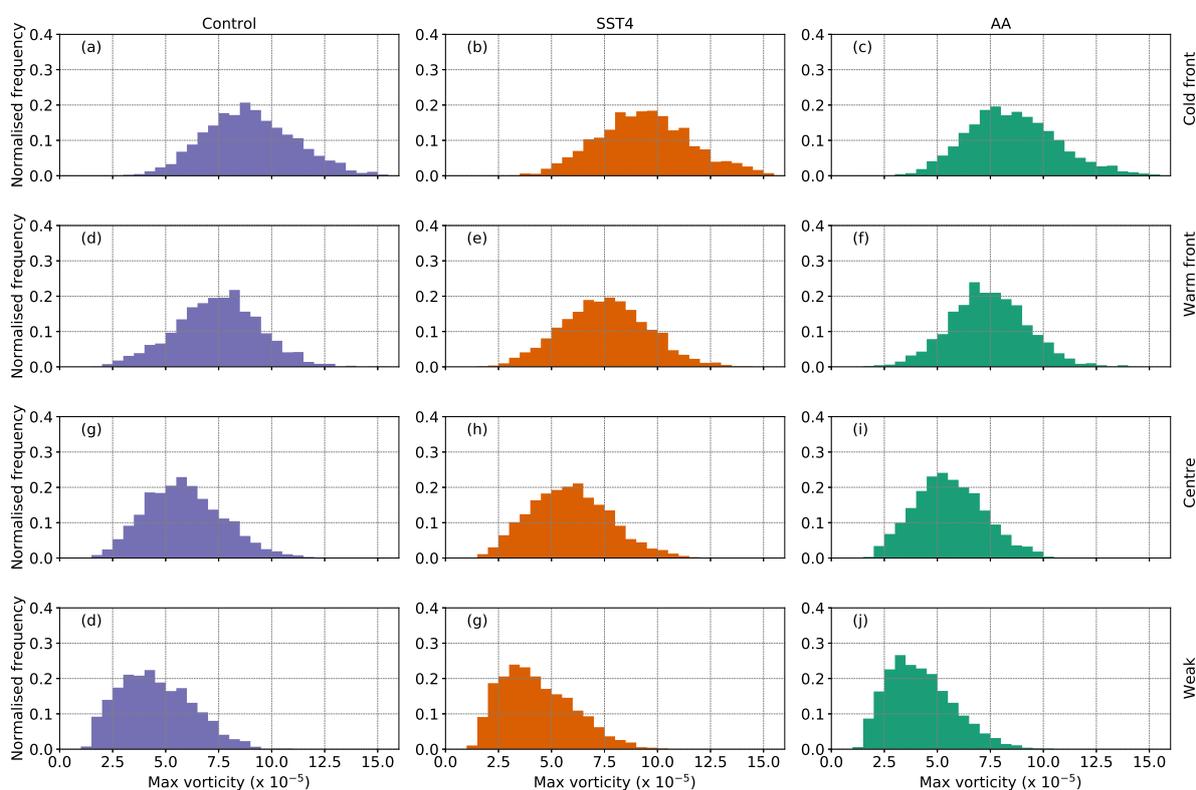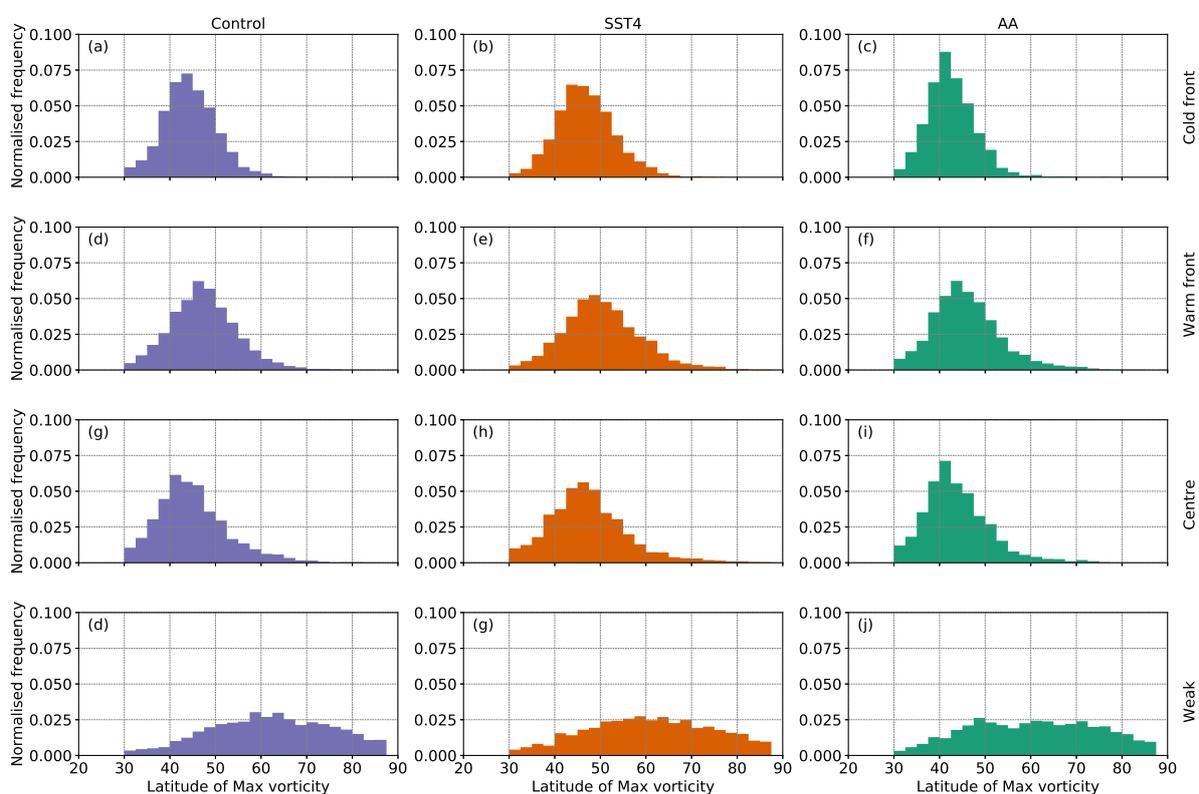
Figure 8. Probability density distributions of the maximum 850-hPa vorticity (T42 values) for each cluster (different rows) and each experiment (different columns). Cyclones are only included if they exist 24 hours before the time of maximum vorticity and reach their maximum vorticity poleward of $30°$ N.

Figure 9. Probability density distributions of the latitude of the the maximum 850-hPa vorticity for each cluster (different rows) and each experiment (different columns). Cyclones are only included if they exist 24 hours before the time of maximum vorticity and reach their maximum vorticity poleward of $30°$N.
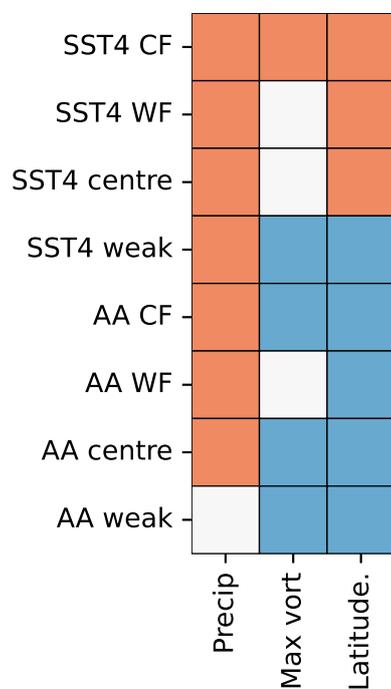
Figure 10. Summary of statistically significant differences between each cluster's precipitation, maximum vorticity, and latitudes of maximum vorticity and the corresponding cluster in the control simulation. Orange (blue) indicates that the cluster as labelled on the y-axis has a statistically larger (smaller) value than in the corresponding cluster in the control simulation. White boxes mean there is no statistically different between the cluster labelled on the y-axis and the corresponding cluster in the control simulation. CF indicates the cold front ETC and WF the warm front ETC.
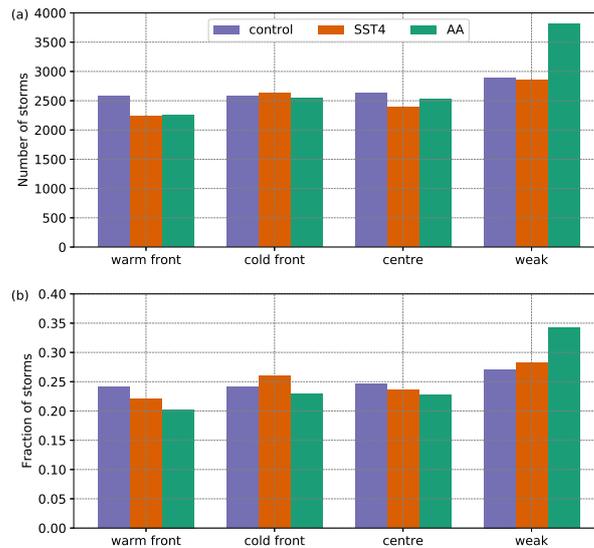
Figure 11. (a) The total number of ETCs in each cluster for each experiment and (b) the relative fraction of ETCs in each cluster for each experiment.
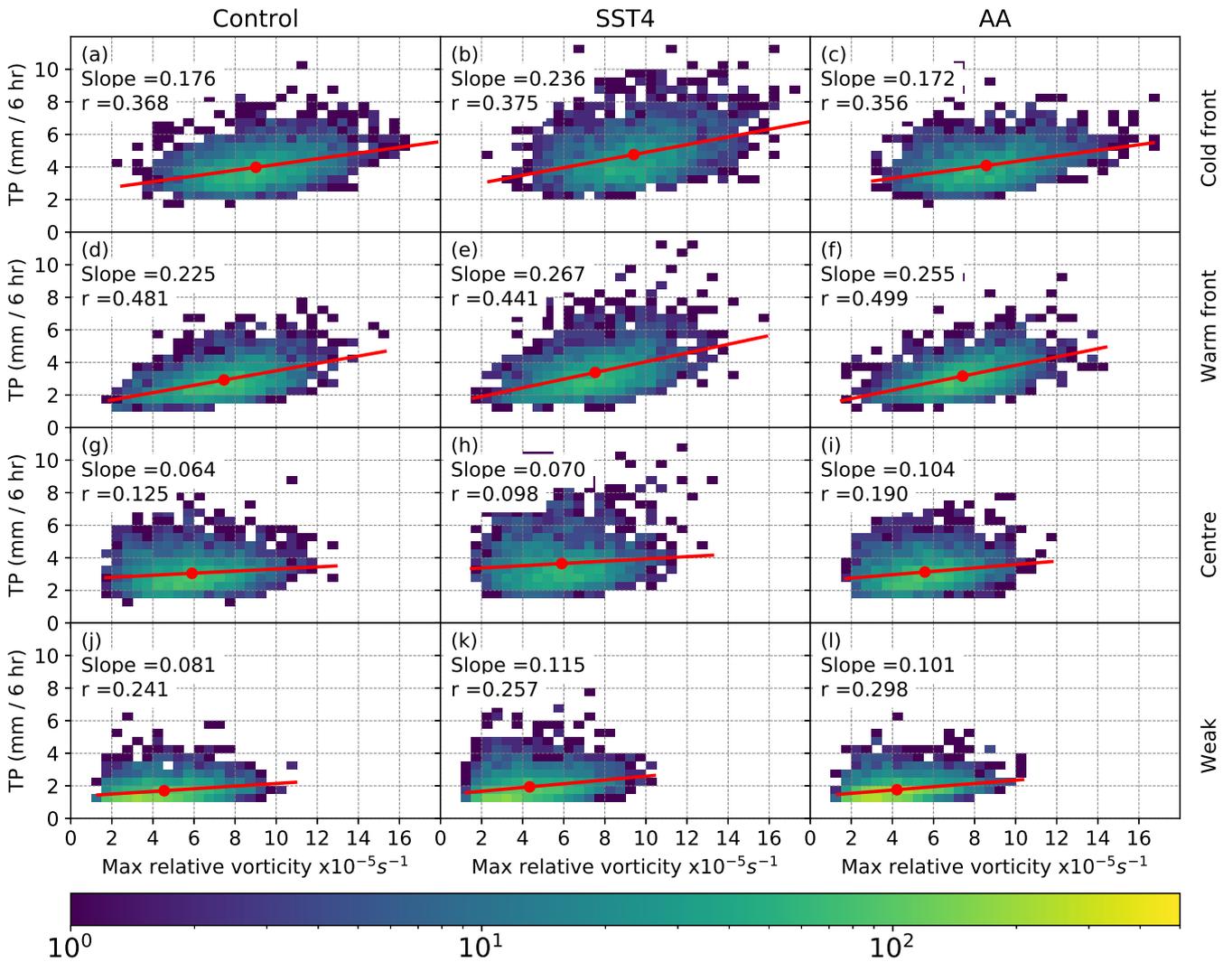
Figure 12. Two-dimensional histograms showing the relation between maximum relative vorticity (T42 values) and ETC-related precipitation 12 hours before the time of maximum relative vorticity for each simulation and each cluster. Precipitation is the area average, averaged over all points with a 12 degree radius of the ETC centre where the rain rate exceeded 1 mm / 6 hr. Only ETCs which exist at -24 hr and have their maximum vorticity north of $30°$N are included.

Table 1. Mean temperature (K) and mean precipitation (mm per day) from all experiments. Values are area / global averages, not ETC-related values.

Diagnostic	Control	SST4	AA
Global mean 2-m temperature	286.7	290.8	287.8
Global mean precipitation	3.18	3.63	3.17
25N - 70N mean 2-m temperature	280.1	284.2	281.7
25N - 70N mean precipitation	2.56	2.90	2.62

Table 2. ETC statistics from the control, SST4 and AA experiments. Relative vorticity values have units of $\times\ 10^{-5}\mathrm{s}^{-1}$ and latitudes are degrees North. ETCs are only included if they exist 24 hours before time of maximum vorticity and reach their maximum vorticity north of $30°$N

Diagnostic	Control	SST4	AA
Number of ETCs	10669	10121	11139
Median number of ETCs per year $\pm$ 1 std	1133 ± 16.4	1134 ± 24.3	1160 ± 14.2
Mean maximum 850-hPa vorticity	6.66	6.66	6.14
Median maximum 850-hPa vorticity	6.53	6.50	5.97
Standard deviation of maximum 850-hPa vorticity	2.56	2.71	2.45
Percentage of cyclones with max vort $> 10\times 10^{-5}\mathrm{s}^{-1}$	10.3%	12.1%	6.7%
median genesis latitude	43.6	45.3	42.7
median latitude of maximum vorticity	47.3	49.6	46.2
median lysis latitude	51.2	53.1	49.8

Table 3. Slope values (units of (mm / 6 hr) s) and correlations coefficients between maximum vorticity (T42 values) and ETC precipitation at different offset times for each experiment

offset time	Control		SST4		AA	
	slope	r	slope	r	slope	r
-72 hr	0.204	0.363	0.241	0.352	0.202	0.352
-48 hr	0.247	0.474	0.290	0.459	0.263	0.526
-24 hr	0.261	0.566	0.319	0.561,	0.298	0.615
-12 hr	0.275	0.586	0.331	0.574	0.311	0.635
0 hr	0.227	0.504	0.258	0.483	0.254	0.561
+24 hr	0.108	0.282	0.121	0.278	0.129	0.354

Code availability. OpenIFS is available under license from the European Centre for Medium Range Weather Forecasting (ECMWF). See https://confluence.ecmwf.int/display/OIFS for more details. TRACK-1.5.2 is available at https://gitlab.act.reading.ac.uk/track/track

Author contributions. VAS and JLC designed the study. VAS performed the experiments, and did most of the data analysis and writing. Both
525 authors contributed equally to the interpretation of the results.

Competing interests. There are no competing interests

References

Binder, H., Boettcher, M., Joos, H., and Wernli, H.: The role of warm conveyor belts for the intensification of extratropical cyclones in Northern Hemisphere winter, J. Atmos. Sci., 73, 3997–4020, https://doi.org/10.1175/JAS-D-15-0302.1, 2016.

Binder, H., Joos, H., Sprenger, M., and Wernli, H.: Warm conveyor belts in present-day and future climate simulations. Part II: Role of potential vorticity production for cyclone intensification, Weather Clim. Dynam. Discuss., https://doi.org/10.5194/wcd-2022-37, in review, 2022.

Bjerknes, J.: On the structure of moving cyclones, Mon. Wea. Rev., 47, 95–99, 1919.

Bjerknes, J. and Solberg, H.: Life cycle of cyclones and the polar front theory of atmospheric circulation, Geofys. Publ., 3, 1–1, 1922.

Booth, J. F., Naud, C. M., and Jeyaratnam, J.: Extratropical Cyclone Precipitation Life Cycles: A Satellite-Based Analysis, Geophys. Res. Lett., 45, 8647–8654, https://doi.org/10.1029/2018GL078977, 2018.

Boutle, I. A., Belcher, S. E., and Plant, R. S.: Moisture transport in midlatitude cyclones, Quart. J. Roy. Meteor. Soc., 137, 360–373, https://doi.org/10.1002/qj.783, 2011.

Browning, K. A.: Radar measurements of air motion near fronts, Weather, 26, 320–340, https://doi.org/10.1002/j.1477-8696.1971.tb04211.x, 1971.

Carlson, T. N.: Airflow through midlatitude cyclones and the comma cloud pattern, Mon. Wea. Rev., 108, 1498–1509, https://doi.org/10.1175/1520-0493(1980)108<1498:ATMCAT>2.0.CO;2, 1980.

Catto, J. L.: Extratropical cyclone classification and its use in climate studies, Rev. Geophys., 54, 486–520, https://doi.org/10.1002/2016RG000519, 2016.

Catto, J. L.: A New Method to Objectively Classify Extratropical Cyclones for Climate Studies: Testing in the Southwest Pacific Region, J. Climate, 31, 4683 – 4704, https://doi.org/10.1175/JCLI-D-17-0746.1, 2018.

Catto, J. L. and Pfahl, S.: The importance of fronts for extreme precipitation, J. Geophys. Res., 118, 10,791–10,801, https://doi.org/10.1002/jgrd.50852, 2013.

Catto, J. L., Shaffrey, L. C., and Hodges, K. I.: Can climate models capture the structure of extratropical cyclones?, J. Climate, 23, 1621–1635, https://doi.org/10.1175/2009JCLI3318.1, 2010.

Catto, J. L., Jakob, C., Berry, G., and Nicholls, N.: Relating global precipitation to atmospheric fronts, Geophys. Res. Lett., 39, https://doi.org/10.1029/2012GL051736, 2012.

Catto, J. L., Madonna, E., Joos, H., Rudeva, I., and Simmonds, I.: Global Relationship between Fronts and Warm Conveyor Belts and the Impact on Extreme Precipitation, J. Climate, 28, 8411 – 8429, https://doi.org/10.1175/JCLI-D-15-0171.1, 2015.

Choudhary, A. and Voigt, A.: Impact of grid spacing, convective parameterization and cloud microphysics in ICON simulations of a warm conveyor belt, Weather Clim. Dynam. 3, 1199–1214, https://doi.org/10.5194/wcd-3-1199-2022, 2022.

Dacre, H. F. and Gray, S. L.: The spatial distribution and evolution characteristics of North Atlantic cyclones, Mon. Wea. Rev., 137, 99–115, https://doi.org/10.1175/2008MWR2491.1, 2009.

Dacre, H. F., Hawcroft, M. K., Stringer, M. A., and Hodges, K. I.: An extratropical cyclone atlas: A tool for illustrating cyclone structure and evolution characteristics, Bull. Amer. Meteor. Soc., 93, 1497–1502, https://doi.org/10.1175/BAMS-D-11-00164.1, 2012.

Dai, P. and Nie, J.: A global quasigeostrophic diagnosis of extratropical extreme precipitation, J. Climate, 33, 9629–9642, https://doi.org/10.1175/JCLI-D-20-0146.1, 2020.

Dai, P. and Nie, J.: Robust expansion of extreme midlatitude storms under global warming, Geophys. Res. Lett., p. e2022GL099007, https://doi.org/10.1029/2022GL099007, 2022.

Dolores-Tesillos, E., Teubler, F., and Pfahl, S.: Future changes in North Atlantic winter cyclones in CESM-LE – Part 1: Cyclone intensity,
570   potential vorticity anomalies, and horizontal wind speed, Weather Clim. Dynam. 3, 429–448, https://doi.org/10.5194/wcd-3-429-2022, 2022.

Douville, H., Raghavan, K., Renwick, J., Allan, R., Arias, P., Barlow, M., Cerezo-Mota, R., Cherchi, A., Gan, T., Gergis, J., Jiang, D., Khan, A., Pokam Mba, W., Rosenfeld, D., Tierney, J., and Zolina, O.: Water Cycle Changes, p. 1055–1210, Cambridge University Press, Cambridge, United Kingdom and New York, NY, USA, https://doi.org/10.1017/9781009157896.010, 2021.

575 Evans, M. S., Keyser, D., Bosart, L. F., and Lackmann, G. M.: A Satellite-Derived Classification Scheme for Rapid Maritime Cyclogenesis, Mon. Wea. Rev., 122, 1381 – 1416, https://doi.org/10.1175/1520-0493(1994)122<1381:ASDCSF>2.0.CO;2, 1994.

Field, P. R. and Wood, R.: Precipitation and cloud structure in midlatitude cyclones, J. Climate, 20, 233–254, https://doi.org/10.1175/JCLI3998.1, 2007.

Harrold, T. W.: Mechanisms influencing the distribution of precipitation within baroclinic disturbances, Quart. J. Roy. Meteor. Soc., 99,
580   232–251, https://doi.org/10.1002/qj.49709942003, 1973.

Hartmann, D. L.: Global Physical Climatology, vol. 103, Elsevier, 2015.

Hawcroft, M., Walsh, E., Hodges, K., and Zappa, G.: Significantly increased extreme precipitation expected in Europe and North America from extratropical cyclones, Environmental Research Letters, 13, 124 006, https://doi.org/10.1088/1748-9326/aaed59, 2018.

Hawcroft, M. K., Shaffrey, L. C., Hodges, K. I., and Dacre, H. F.: How much Northern Hemisphere precipitation is associated with extrat-
585   ropical cyclones?, Geophys. Res. Lett., 39, https://doi.org/10.1029/2012GL053866, 2012.

Held, I. M. and Soden, B. J.: Robust responses of the hydrological cycle to global warming, J. Climate, 19, 5686–5699, https://doi.org/10.1175/JCLI3990.1, 2006.

Hodges, K. I.: A general method for tracking analysis and its application to meteorological data, Mon. Wea. Rev., 122, 2573–2586, https://doi.org/10.1175/1520-0493(1994)122<2573:AGMFTA>2.0.CO;2, 1994.

590 Hodges, K. I.: Feature tracking on the unit sphere, Mon. Wea. Rev., 123, 3458–3465, https://doi.org/10.1175/1520-0493(1995)123<3458:FTOTUS>2.0.CO;2, 1995.

Hodges, K. I., Lee, R. W., and Bengtsson, L.: A comparison of extratropical cyclones in recent reanalyses ERA-Interim, NASA MERRA, NCEP CFSR, and JRA-25, J. Climate, 24, 4888–4906, https://doi.org/10.1175/2011JCLI4097.1, 2011.

Kirshbaum, D., Merlis, T., Gyakum, J., and McTaggart-Cowan, R.: Sensitivity of idealized moist baroclinic waves to environmental temper-
595   ature and moisture content, J. Atmos. Sci., 75, 337–360, https://doi.org/10.1175/JAS-D-17-0188.1, 2018.

Kodama, C., Iga, S., and Satoh, M.: Impact of the sea surface temperature rise on storm-track clouds in global nonhydrostatic aqua planet simulations, Geophys. Res. Lett., 41, 3545–3552, https://doi.org/10.1002/2014GL059972, https://agupubs.onlinelibrary.wiley.com/doi/abs/10.1002/2014GL059972, 2014.

Kodama, C., Stevens, B., Mauritsen, T., Seiki, T., and Satoh, M.: A new perspective for future precipitation change from intense extratropical
600   cyclones, Geophys. Res. Lett., 46, 12 435–12 444, https://doi.org/10.1029/2019GL084001, 2019.

Lloyd, S.: Least squares quantization in PCM, IEEE transactions on information theory, 28, 129–137, https://doi.org/10.1109/TIT.1982.1056489, 1982.

Madonna, E., Wernli, H., Joos, H., and Martius, O.: Warm Conveyor Belts in the ERA-Interim Dataset (1979–2010). Part I: Climatology and Potential Vorticity Evolution, J. Climate, 27, 3 – 26, https://doi.org/10.1175/JCLI-D-12-00720.1, 2014.

605   Michaelis, A. C., Willison, J., Lackmann, G. M., and Robinson, W. A.: Changes in Winter North Atlantic Extratropical Cyclones in High-Resolution Regional Pseudo – Global Warming Simulations, J. Climate, 30, 6905–6925, https://doi.org/10.1175/JCLI-D-16-0697.1, 2017.

Milrad, S. M., Atallah, E. H., and Gyakum, J. R.: Synoptic typing of extreme cool-season precipitation events at St. John's, Newfoundland, 1979–2005, Weather and Forecasting, 25, 562–586, https://doi.org/10.1175/2009WAF2222301.1, 2010.

Neale, R. B. and Hoskins, B. J.: A standard test for AGCMs including their physical parametrizations: I: The proposal, Atmospheric Science
610   Letters, 1, 101–107, https://doi.org/10.1006/asle.2000.0022, 2000.

Owen, L. E., Catto, J. L., Stephenson, D. B., and Dunstone, N. J.: Compound precipitation and wind extremes over Europe and their relationship to extratropical cyclones, Weather and Climate Extremes, 33, 100 342, https://doi.org/https://doi.org/10.1016/j.wace.2021.100342, 2021.

Owen, L. E., Catto, J. L., Stephenson, D. B., and Dunstone, N. J.: in prep.

615   Pedregosa, F., Varoquaux, G., Gramfort, A., Michel, V., Thirion, B., Grisel, O., Blondel, M., Prettenhofer, P., Weiss, R., Dubourg, V., et al.: Scikit-learn: Machine learning in Python, the Journal of machine Learning research, 12, 2825–2830, 2011.

Pfahl, S. and Sprenger, M.: On the relationship between extratropical cyclone precipitation and intensity, Geophys. Res. Lett., 43, 1752–1758, https://doi.org/10.1002/2016GL068018, 2016.

Pfahl, S. and Wernli, H.: Quantifying the Relevance of Cyclones for Precipitation Extremes, J. Climate, 25, 6770 – 6780,
620   https://doi.org/10.1175/JCLI-D-11-00705.1, 2012.

Pfahl, S., Madonna, E., Boettcher, M., Joos, H., and Wernli, H.: Warm Conveyor Belts in the ERA-Interim Dataset (1979–2010). Part II: Moisture Origin and Relevance for Precipitation, J. Climate, 27, 27 – 40, https://doi.org/10.1175/JCLI-D-13-00223.1, 2014.

Pfahl, S., O'Gorman, P. A., and Singh, M. S.: Extratropical cyclones in idealized simulations of changed climates, J. Climate, 28, 9373–9392, https://doi.org/10.1175/JCLI-D-14-00816.1, 2015.

625   Priestley, M. D. and Catto, J. L.: Future changes in the extratropical storm tracks and cyclone intensity, wind speed, and structure, Weather Clim. Dynam. 3, 337–360, https://doi.org/10.5194/wcd-3-337-2022, 2022.

Priestley, M. D., Ackerley, D., Catto, J. L., Hodges, K. I., McDonald, R. E., and Lee, R. W.: An overview of the extratropical storm tracks in CMIP6 historical simulations, J. Climate, 33, 6315–6343, https://doi.org/10.1175/JCLI-D-19-0928.1, 2020.

Rantanen, M., Räisänen, J., Sinclair, V. A., and Järvinen, H.: Sensitivity of idealised baroclinic waves to mean atmospheric temperature and
630   meridional temperature gradient changes, Climate Dyn., 52, 2703–2719, https://doi.org/10.1007/s00382-018-4283-3, 2019.

Reboita, M. S., Reale, M., da Rocha, R. P., Giorgi, F., Giuliani, G., Coppola, E., Nino, R. B. L., Llopart, M., Torres, J. A., and Cavazos, T.: Future changes in the wintertime cyclonic activity over the CORDEX-CORE southern hemisphere domains in a multi-model approach, Climate Dyn., 57, 1533–1549, https://doi.org/10.1007/s00382-020-05317-z, 2021.

Rousseeuw, P. J.: Silhouettes: a graphical aid to the interpretation and validation of cluster analysis, Journal of computational and applied
635   mathematics, 20, 53–65, https://doi.org/10.1016/0377-0427(87)90125-7, 1987.

Shapiro, M. A. and Keyser, D.: Fronts, jet streams and the tropopause., in: Extratropical Cyclones, The Erik Palmén Memorial Volume, pp. 167–191, Amer. Meteor. Soc, 1990.

Simmons, A. J. and Hoskins, B. J.: The life cycles of some nonlinear baroclinic waves, J. Atmos. Sci., 35, 414–432, https://doi.org/10.1175/1520-0469(1978)035<0414:TLCOSN>2.0.CO;2, 1978.

640   Sinclair, M. R. and Revell, M. J.: Classification and Composite Diagnosis of Extratropical Cyclogenesis Events in the Southwest Pacific, Mon. Wea. Rev., 128, 1089 – 1105, https://doi.org/10.1175/1520-0493(2000)128<1089:CACDOE>2.0.CO;2, 2000.

Sinclair, V. A., Rantanen, M., Haapanala, P., Räisänen, J., and Järvinen, H.: The characteristics and structure of extra-tropical cyclones in a warmer climate, Weather Clim. Dynam. 1, 1–25, https://doi.org/10.5194/wcd-1-1-2020, 2020.

Thorncroft, C., Hoskins, B., and McIntyre, M.: Two paradigms of baroclinic-wave life-cycle behaviour, Quart. J. Roy. Meteor. Soc., 119,

645 17–55, https://doi.org/10.1002/qj.49711950903, 1993.

Yettella, V. and Kay, J. E.: How will precipitation change in extratropical cyclones as the planet warms? Insights from a large initial condition climate model ensemble, Climate Dyn., 49, 1765–1781, https://doi.org/10.1007/s00382-016-3410-2, 2017.

Zhang, Z. and Colle, B. A.: Impact of Dynamically Downscaling Two CMIP5 Models on the Historical and Future Changes in Winter Extratropical Cyclones along the East Coast of North America, J. Climate, 31, 8499 – 8525, https://doi.org/10.1175/JCLI-D-18-0178.1,

650 2018.